Journal of Zhejiang University-SCIENCE A (Applied Physics & Engineering)
ISSN 1673-565X (Print); ISSN 1862-1775 (Online)
www.zju.edu.cn/jzus; www.springerlink.com
E-mail: jzus@zju.edu.cn

Bearing capacity and load transfer mechanism of a static drill rooted nodular pile in soft soil areas

Jia-jin ZHOU[†1], Kui-hua WANG[†‡1], Xiao-nan GONG[1], Ri-hong ZHANG[2]

([1]*Research Center of Coastal and Urban Geotechnical Engineering, Zhejiang University, Hangzhou 310058, China*)

([2]*ZDOON Building Material Group, Ningbo 315000, China*)

[†]E-mail: zjjmuforever@163.com; zdwkh0618@zju.edu.cn

Received Apr. 11, 2013; Revision accepted July 30, 2013; Crosschecked Sept. 12, 2013

Abstract: The static drill rooted nodular pile is a new type of pile foundation consisting of precast nodular pile and the surrounding cemented soil. This composite pile has a relatively high bearing capacity and the mud pollution will be largely reduced during the construction process by using this type of pile. In order to investigate the bearing capacity and load transfer mechanism of this pile, a group of experiments were conducted to provide a comparison between this new pile and the bored pile. The axial force of a precast nodular pile was also measured by the strain gauges installed on the pile to analyze the distribution of the axial force of the nodular pile and the skin friction supported by the surrounding soil, then 3D models were built by using the ABAQUS finite element program to investigate the load transfer mechanism of this composite pile in detail. By combining the results of field tests and the finite element method, the outcome showed that the bearing capacity of a static drill rooted nodular pile is higher than the bored pile, and that this composite pile will form a double stress dispersion system which will not only confirm the strength of the pile, but also make the skin friction to be fully mobilized. The settlement of this composite pile is mainly controlled by the precast nodular pile; meanwhile, the nodular pile and the surrounding cemented soil can be considered as deformation compatibility during the loading process. The nodes on the nodular pile play an important role during the load transfer process, the shear strength of the interface between the cemented soil and the soil of the static drill rooted pile is larger than that of the bored pile.

Key words: Static drill rooted nodular pile, Load transfer, Bearing capacity, ABAQUS, Double stress dispersion system, Three-dimensional modeling

doi:10.1631/jzus.A1300139 **Document code:** A **CLC number:** TU47

1 Introduction

Nowadays, precast reinforced concrete piles and bored piles are widely used in high-rise building engineering in the deep soft soil areas in China. The precast reinforced concrete pile has the advantages of fast piling speed and relatively low cost, while the superiorities of the bored pile are relatively high bearing capacity, controlling the construction depth easily and making little noise. However, these two types of piles also have obvious shortages in practical applications. The skin friction of precast reinforced concrete piles is always small when used in the soft soil foundation, and it often occurs that the skin friction reaches the ultimate state and the settlement becomes so large that the pile cannot continue to bear the load while the strength of the pile is not mobilized fully, which leads to a waste of the strength of the pile material. Moreover, the construction method of the precast reinforced concrete pile will produce a severe compaction effect and have an effect on the surrounding piles and facilities. The bored pile has a mud skin effect and pile tip sediment problems which will lead to the decline of the bearing capacity, and a large amount of mud is produced during the construction process, which will cause serious pollution to the environment.

Therefore, it is hoped that a new type of pile can be created to replace the above mentioned two piles.

[‡]Corresponding author

The static drill rooted nodular pile has been identified as a pile that can be used in the deep soft soil area in China in these conditions. It was first used in Japan and then introduced into China. The static drill rooted nodular pile consists of a precast nodular pile and cemented soil. Firstly, a helical auger is used for stirring and grouting to form cemented soil, then the precast nodular pile is put into the cemented soil. This construction method not only avoids the compaction effect which occurs in the driving process of precast pile, but also averts the mud skin effect and pile tip sediment problems in the construction process of the bored pile. The static drill rooted nodular pile has been used in certain places of deep soft soil layers in Zhejiang province, China, and statistics from these primary applications show that the cost can be decreased by 10% by using this nodular pile approach compared to the bored piles. Therefore, this composite pile not only avoids the soil compaction effect and mud pollution, but also has advantages of economy, so it is of great significance to introduce this pile to the broad soft soil areas in China. Whereas almost no studies on the load transfer mechanism and calculating method have been carried on in China, due to different geological conditions, researches conducted by Japanese (Yabuuchi, 1994; Horiguchi and Karkee, 1995; Borda *et al.*, 2007; Karkee *et al.*, 1998; Honda *et al.*, 2011) do not necessarily apply to the soft soil area in China, and studies on other composite piles (Petros *et al.*, 1994; Wang *et al.*, 1998; Dong *et al.*, 2004) can be of some help for the research of the nodular pile, while the research results of these composite piles can not wholly apply to the nodular piles.

In this study, full-scale destructive field tests of static drill rooted modular piles and bored piles were carried out to compare the bearing capacity between these two piles, full-scale field tests of static drill rooted piles attached with strain gauges were also conducted to investigate the load transfer mechanism of static drill rooted piles. Finally, a finite element program, ABAQUS, was used to simulate the piles in the field tests for deep analysis of the static drill rooted pile.

2 Bearing capacity of a nodular pile

2.1 Static drill rooted method

The static drill rooted method is a type of environmentally friendly construction method, which can largely decrease the mud emissions and have a small effect on the surrounding facilities. The construction process can be concluded in the following five steps:

1. Drilling: position the drill machine at the right place, then the drilling speed is confirmed according to the geological conditions. In addition, during the drilling process, a water or bentonite mixture liquid is injected to repair the hole according to the geological conditions.

2. Expanding: the drill machine used here is special and has a wing that can expand. When the drill machine reaches the set depth, the wing expands as the set size and makes the diameter of the hole at the bottom expand, and the whole process is monitored by the management device.

3. Grouting at pile tip: grouting at pile tip, lift the drill machine up and down repeatedly during the grouting process to ensure that the cement paste is injected into the bottom of the hole and the cemented soil is uniform.

4. Grouting and pulling out the drill machine: grouting along the hole and stirring repeatedly while pulling out the drilling machine.

5. Put the pile into the hole: put the precast nodular pile into the hole after the drill machine is pulled out. The process is monitored to ensure that the pile is vertical and reaches the right depth.

The specific construction process of a static drill rooted nodular pile is shown in Fig. 1.

2.2 Load transfer mechanism of a nodular pile element

The static drill rooted nodular pile is a composite pile foundation that consists of precast nodular pile and the surrounding cemented soil. Therefore, it is different from the traditional piles, which causes its load transfer mechanism to be different. The vertical load is mainly born by the precast nodular pile, then the precast pile transmits part of the load to the cemented soil, and the cemented soil transmits the load to the surrounding soil. The cemented soil makes a big difference during the loading process, and from the sample of actual engineering, the compressive strength of the cemented paste is 10 MPa to 20 MPa As the strength of the cemented soil is largely dependent on the soil, the compressive strength of the cemented soil is 4 MPa to 7 MPa in the current actual

engineering. The sketch of the nodular pile and the load transfer path of a pile element are shown in Fig. 2. In this figure, the precast nodular pile is surrounded by cemented soil, and the tip type of the nodular pile is opened. Q_1 is the axial force on the precast nodular pile, Q_1' and Q_1'' are the axial forces on the external cemented soil and internal cemented soil, respectively. q_{s1} is the side friction between the nodular pile and internal cemented soil, q_{s2} is the side friction between the nodular pile and external cemented soil, and q_{s3} is the side friction between the external cemented soil and surrounding soil. The relationship between these parameters can be summarized as follows:

$$Q_1 = Q_2 + q_{s1}u_1L + q_{s2}u_2L, \tag{1}$$

$$Q_1' + q_{s2}u_2L = Q_2' + q_{s3}u_3L, \tag{2}$$

$$Q_1'' + q_{s1}u_1L = Q_2'', \tag{3}$$

where u_1 and u_2 are the internal and external perimeter of the nodular pile, u_3 is the perimeter of the cemented soil, and L is the length of the pile element.

2.3 Site conditions and pile conditions

To investigate the bearing capacity of the static drill rooted nodular piles and to compare the bearing capacity of nodular piles and bored piles, destructive field tests of four static drill rooted nodular piles and two bored piles were carried out.

Two types of nodular piles were selected in this field test, i.e., one type had a diameter of 650 mm in the node and 500 mm in the other parts (called 650 (500) mm type), the other type had a diameter of 800 mm in the node and 600 mm in the other parts (called 800 (600) mm type). The diameters of the two bored piles were 800 mm and 1000 mm, respectively, and all six piles were 64 m long. In this test, the nodular piles and normal precast pipe piles were welded together. The nodes on the nodular pile are to strengthen the cohesion between the pile and cemented soil, in the shallow soil layer, for the cohesion between cemented soil and soil is relatively small, so the cohesion between pile and cemented soil need not be very high and pipe piles are selected for the shallow soil layer. The 650 (500) mm type nodular piles were connected with three 600 mm pipe piles each with a length of 12 m, 12 m, and 10 m, and two 650 (500) mm nodular piles of 15 m were welded beneath the pipe piles, so the total length was 64 m, and the diameter of the drill hole was 700 mm. Two 800 (600) mm

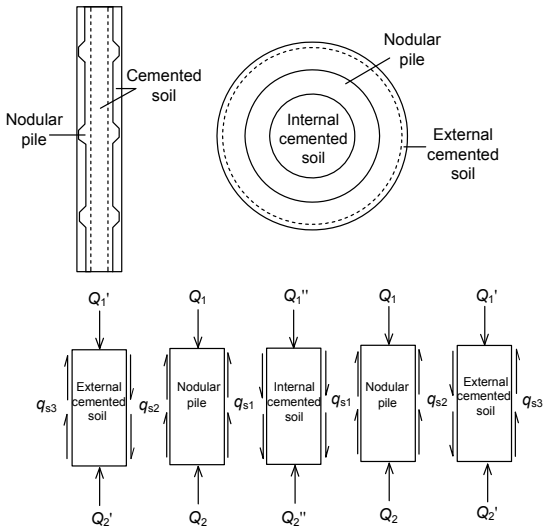

Fig. 2 Sketch of nodular pile and load transfer path of a pile element

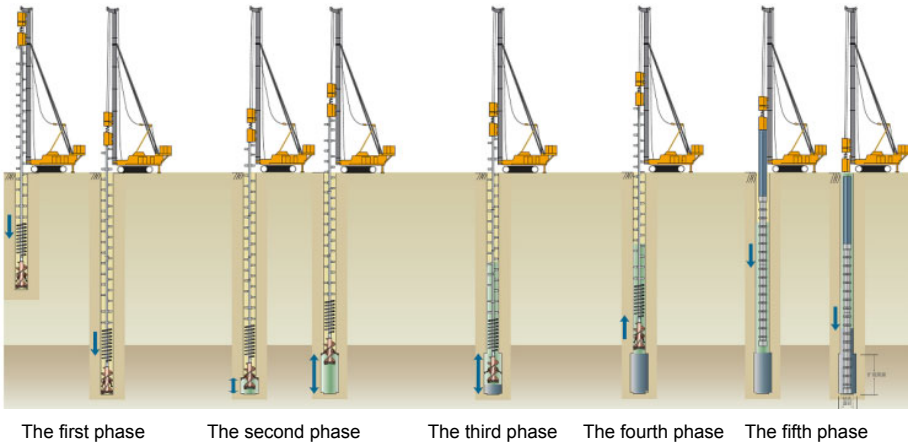

Fig. 1 Construction process of static drill rooted nodular pile

nodular piles each with a length of 15 m were connected with three 800 mm pipe piles each with a length of 4 m, 15 m, and 15 m, the total length was 64 m, and the diameter of the drill hole was 850 mm. The sketch of the test piles and the layout of six piles in this test are shown in Fig. 3. The drill diameter of the No. 1 and No. 2 test piles is 850 mm, and that of the No. 3 and No. 4 test piles is 700 mm. The diameter of the No. 5 test piles is 1000 mm and that of the No.6 pile is 800 mm. The detailed soil profiles and properties are given in Table 1, in which γ_{sat} is the saturated unit weight; I_P and I_L are the plasticity index and liquidity index; E_s is the compression modulus of each soil layer; c and φ are the cohesion and the internal friction angle of each soil layer, which are measured by consolidated undrained (CU) triaxial tests; q_{sa} and q_{pa} are the recommended values of the ultimate unit side friction and the tip resistance, respectively, which are estimated from the CPTs.

2.4 Single pile field tests

Single pile field tests were conducted according to the industry standard in China (JGJ106-2003). A slow maintained load method was adopted for the field tests, and the load was applied step by step. The value of a step was set to 1/8–1/12 of the estimated maximum testing load, and the value of the first step was twice that of the other steps. Settlements at the pile top were measured at an interval of 5 min, 15 min, 30 min, 45 min, 60 min, 90 min and so on after every loading step until a certain rate of settlement was achieved (e.g., the settlement was not greater than 0.1 mm within every 1 h). The value of unloading was twice that of the loading value and the pile top settlements were measured at an interval of 15 min, 30 min, 60 min, etc. It is necessary to wait for 3 h after unloading to arrive at zero. Figs. 4 and 5 show the load-displacement curves of static drill rooted nodular piles and bored piles.

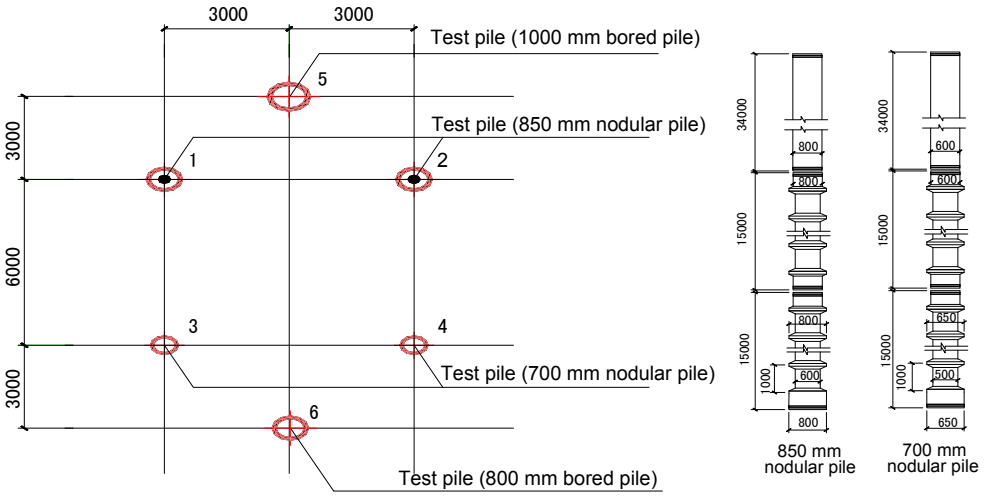

Fig. 3 Sketch of test piles and layout of six piles in this test (unit: mm)

Table 1 Soil profiles and properties in test site

Layer No.	Soil layer	Thickness of soil layer (m)	γ_{sat} (kN/m^3)	I_P	I_L	C (kPa)	φ (°)	E_s (MPa)	Pipe pile		Bored pile		Standard penetration test blow count
									q_{sa} (kPa)	q_{pa} (kPa)	q_{sa} (kPa)	q_{pa} (kPa)	
1	Saturated silty clay	18.10–18.90	17.5	18.5	1.24	12.0	10.2	2.36	11		8		1
2	Silt	4.10–4.30							18		15		9
3	Saturated silty clay	21.80–22.50	17.9	17.1	1.27	15.4	11.6	3.17	12		9		8
4	Silt clay	2.90–3.20	19.9	12.9	0.45	44.6	17.1	6.97	35		28		10
5	Silt clay	8.50–9.20	18.9	14.6	0.97	20.1	13.3	3.88	25		20		16
6	Silt	3.80–4.70							42		36		55
7	Silt clay	0.90–1.40	20.1	10.5	0.77	26.7	17.1	5.87	25		20		60
8	Silt	5.80–5.90							42	2300	36	550	60

Fig. 4 shows the load-displacement curves of 700 mm nodular piles (as mentioned above, the precast nodular pile is surrounded by cemented soil, and the drill diameter of 650 (500) mm nodular pile is 700 mm, so here they are called 700 mm nodular piles) and 800 mm bored piles. The three load-displacement curves appear to be similar and all have obvious turning points, which indicate that punching failures are likely to occur for all three piles. The failure criteria for three piles are summarized as follows. When the applied load at the No. 3 test pile comes to 8000 kN, the settlement at the pile top sharply increases, the punching failure is thereby very likely to occur; therefore, the ultimate bearing capacity of the No. 3 test pile is 7200 kN. When the No. 4 test pile is loaded to 8600 kN, the settlement at the pile top increases rapidly, the punching failure is thereby very likely to occur, and the ultimate bearing capacity of the No. 4 test pile is 8100 kN. When the applied load at the No. 6 test pile comes to 8800 kN, the settlement at the pile top sharply increases, the punching failure is thereby very likely to occur, and the ultimate bearing capacity of the No. 6 test pile is 8000 kN. In actual engineering, the concrete used in the nodular pile is C100 (JGJ94-2008), the resistance of C100 concrete is 100 MPa, and the reduction coefficient is 0.80. For the 650 (500) mm nodular pile, the thickness of the nodular pile is 100 mm, the surface section is about 0.126 m^2, the maximum applied force on the pile top is 8600 kN, and the vertical stress is 68.2 MPa, which is less than 80 MPa, and the load on the nodular pile must be smaller than 8600 kN, so the material used here is considered reliable. In actual engineering, from the excavation piles after the field test, material failure does not occur. The No. 3 and No. 4 test piles are 700 mm static drill rooted nodular piles and the No. 6 test pile is 800 mm bored pile, while the load-displacement curves and the ultimate bearing capacity of these three piles are appear to be similar, so it can be seen from the field tests that the bearing capacity of 700 mm static drill rooted nodular piles and 800 mm bored piles are similar.

The load-displacement curves of the 850 mm nodular piles (the 800 (600) nodular pile are surrounded by cemented soil with a diameter of 850 mm, so here they are called 850 mm nodular piles) and 1000 mm bored piles are shown in Fig. 5. It can be seen from Fig. 5 that the load-displacement curves of the three test piles are similar. The failure criteria of the three piles are summarized as follows. When the applied load at the No. 1 test pile comes to 9600 kN, the settlement at the pile top sharply increases, the punching failure is thereby very likely to occur, and the ultimate bearing capacity of the No. 1 test pile is 8800 kN. When the No. 2 test pile is loaded to 10000 kN, the settlement at the top of the pile increases rapidly, the punching failure is thereby very likely to occur, and the ultimate bearing capacity of the No. 2 test pile is 9500 kN. When the applied load at the No. 5 test pile comes to 10400 kN, the settlement at the pile top sharply increases, the punching failure is thereby very likely to occur, and the ultimate bearing capacity of No. 6 test pile is 9600 kN. The concrete used in the nodular is C100, i.e., the resistance of the C100 concrete is 100 MPa. For the 800 (600) mm nodular pile, the thickness of the pile is 110 mm, the surface section is about 0.238 m^2, the maximum applied force is 11000 kN, and the vertical stress is 46.2 MPa, which is less than 80 MPa, then the load on the nodular must be smaller than 11000 kN. Thus, the material used here is considered reliable. The No. 1 and No. 2 test piles are 850 mm static drill rooted nodular

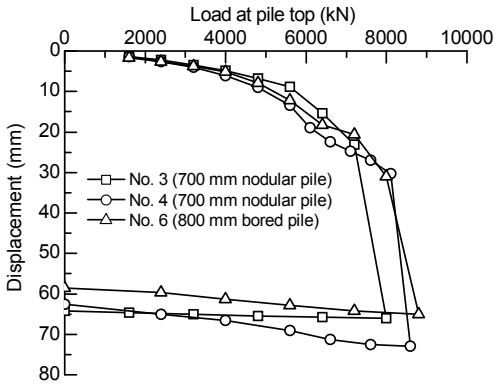

Fig. 4 Load-displacement curves of 700 mm nodular piles and 800 mm bored pile

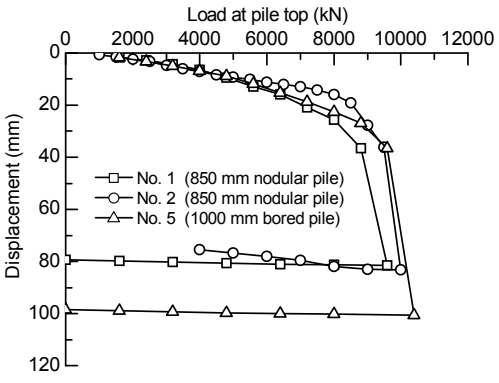

Fig. 5 Load-displacement curves of 850 mm nodular piles and 1000 mm bored pile

piles and the No. 5 test pile is a 1000 mm bored pile. The load-displacement curves and the ultimate bearing capacity of the three test piles are similar as well, so it can also be considered that the bearing capacity of the 850 mm static drill rooted nodular piles and 1000 mm bored piles are similar.

According to the above two groups of field tests, it can be seen that the form of the load-displacement curves of the static drill rooted nodular piles and bored piles are similar. The load applied on the pile top is first provided by the skin friction, and pile tip resistance does not emerge until the skin resistance is fully mobilized; finally, the punching failure occurs at last. However, because of different pile-soil interfaces which are of great importance for developing of the skin friction, the skin friction of the nodular pile is provided by the cemented soil-soil interface, while the skin friction of the bored pile is provided by the pile-soil interface, and the bearing capacity of the nodular pile and bored pile is different. The two groups of field tests show that the bearing capacity of 700 mm static drill rooted nodular piles and 800 mm bored piles are similar, while the bearing capacity of 850 mm static drill rooted nodular piles is similar to 1000 mm bored piles. Therefore, it can be concluded that the bearing capacity of static drill rooted nodular piles is higher than the bored piles.

3 Load transfer mechanism of nodular piles

3.1 Test profile

The field tests were conducted in an expressway engineering project. In order to investigate the load transfer mechanism of static drill rooted nodular piles, a field test of a 72 m long nodular pile attached with strain gauges was carried out. The core precast pile also consisted of pipe piles and nodular piles: three 800 mm pipe piles each with a length of 15 m, 15 m, and 12 m were connected with two 15 m long 800 (600) mm nodular piles, the total length of the pile is 72 m, and the diameter of the drill hole is 850 mm. To measure the axial force of the test pile, the strain gauges were arranged according to soil profiles in the test field, eight cross sections of the pile were attached with strain gauges; each section was attached with two symmetry strain gauges, and totally 16 strain gauges were set.

The field test was conducted according to the industry standard in China (JGJ106-2003). A slow maintained load method was adopted for the field test. The loading system consists of five 3200 kN hydraulic jacka, and a 70 MPa ultrahigh pressure hydraulic system, and oil pump. Statistics were collected by a RS-JYC pile field test tester produced by the Wuhan Yanhai Company, China. The loading and unloading steps were the same as those mentioned in Section 2.3.2. The detailed soil profiles and properties are given in Table 2, and the sketch of strain gauges and a schematic of the field test are shown in Fig. 6.

3.2 Field test results

3.2.1 Load-displacement response of test pile

The load-displacement curve of the test pile is shown in Fig. 7. The load-displacement curve is almost linear at the beginning of the loading period, and then an obvious turning point appears which indicates

Table 2 Soil profiles and properties in test site

Layer No.	Soil layer	Thickness of soil layer (m)	γ_{sat} (kN/m^3)	e	I_P	I_L	Consolidated quick shear		E_s (MPa)	Cone penetration test		Standard value of the skin friction of bored piles q_{ik} (kPa)
							C (kPa)	φ (°)		q_c (MPa)	f_s (kPa)	
1	Clay	5.0	18.4	1.04	19.2	0.75	27.1	12.9	4.70	0.46	12.99	25
2	Saturated silty clay	7.6	17.0	1.46	20.1	1.45	12.1	8.2	2.57	0.45	8.00	13
3	Silty clay 1	8.4	18.4	1.00	13.0	1.22	12.9	11.4	4.23	0.79	12.66	20
4	Silty clay 2	7.3	19.0	0.89	16.2	0.62	34.7	17.8	6.70	1.73	47.70	46
5	Clayey silt 1	4.6	19.0	0.86	7.6	1.16	12.4	30.2	9.84	6.17	100.3	52
6	Clayey silt 2	24.1	19.0	0.87	8.0	1.16	12.7	29.5	10.6	4.52	121.6	50
7	Silty clay mixed gravel	7.4	19.6	0.75	13.4	0.43	42.8	20.6	9.02			60
8	Silty clay mixed sand	3.2	19.7	0.75	14.7	0.37	38.1	20.5	9.51			44
9	Medium sand	7.2	20.1	0.61			9.9	34.0	12.2			78
10	Silty sand	8.2	19.3	0.76			9.8	32.3	10.1			75

that a punching failure is very likely to occur. It is also shown in Fig. 7 that when the applied load comes to 12000 kN, the settlement at the pile top sharply increases, the punching failure is thereby very likely to occur, and the ultimate bearing capacity of the test pile is 10800 kN. Because of the mistakes of the staffs, the head of the test pile was broken when loaded to 12000 kN, so the test cannot continue and it was impossible to conduct the unloading process. Fortunately it does not make much sense for our study for the punching failure has already occurred. The concrete used in the nodular pile is C100, i.e., the resistance of C100 concrete is 100 MPa. For the 800 (600) mm nodular pile, the thickness of the pile is 110 mm, the surface section is about 0.238 m^2, the maximum applied force is 12000 kN, and the vertical stress is 50.5 MPa, which is less than 80 MPa. Thus, the material used here is reliable. In the field test, no material failure phenomenon is found.

3.2.2 Axial force

Using the measured statistics of the strain gauges at a certain depth, the average axial force can be calculated, and the distribution of the axial force along the test pile is shown in Fig. 8. The axial force decreases along the test pile because of the skin friction provided by the surrounding soil. Fig. 8 also shows that when the applied load is small, the axial force at the lower part of the pile is zero and it begins to rise as the applied load increases. When the applied load comes to 10800 kN, the tip resistance is 2566 kN, which represents 23.76%. The different slopes of the curve between different soil layers also indicate that the skin friction has something to do with the properties of the soil.

3.2.3 Skin friction of the test pile

As a kind of composite pile foundation, nodular piles and cemented soil around the pile are considered as a whole in the loading process, and the skin friction is provided by the cemented soil-soil interface. The skin friction along the pile can be calculated as (Dong *et al.*, 1994):

$$f_{si} = \frac{P_i - P_{i+1}}{A_i}, \tag{4}$$

where P_i and P_{i+1} are axial forces of pile sections i and i+1, respectively, and A_i is the lateral area of the pile, namely the lateral area of the cemented soil. The

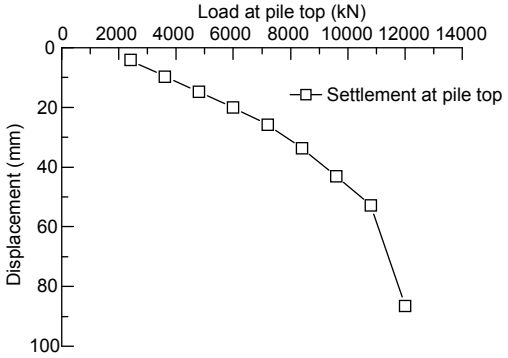

Fig. 7 Load-displacement curve of 850 mm test nodular pile

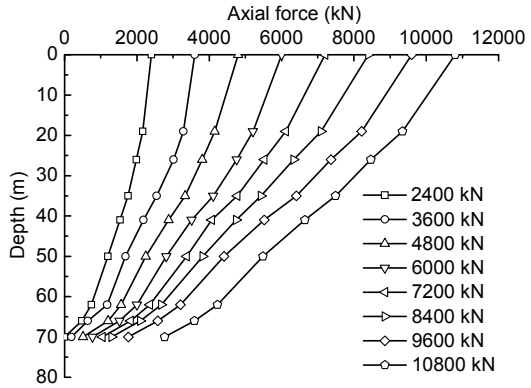

Fig. 8 Axial force of test pile under different loads

(a)

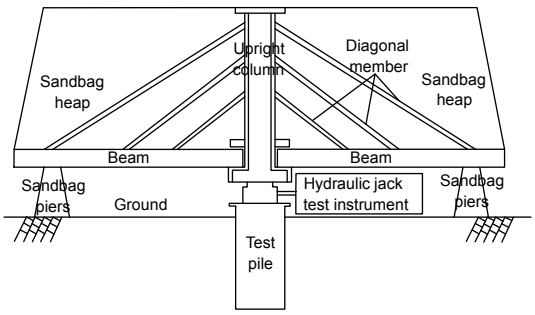

(b)

Fig. 6 Sketch of strain gages attached on pile (a) and schematic of the test (b)

distribution of the skin friction along the test pile is shown in Fig. 9.

Fig. 9 shows that the mobilization of the skin friction is related to the load applied on the pile, the skin friction gradually increases with the increasing applied load before the skin friction is fully mobilized. However, it will have a small reduction with the applied load still increasing in some soil layers after the skin friction is fully mobilized, which is called shaft resistance softening, and strain softening of overpressure soft clay and the dilatancy of the sand may lead to this phenomenon (Zhang, 2007).

It can also be seen in Fig. 9 that the skin friction is mobilized from the pile top to pile tip, and the skin friction at the lower part of the pile is zero when the applied load is small and the upper skin friction is not fully mobilized; therefore, the lower skin friction does not mobilize until the upper skin friction is fully expressed.

3.2.4 Relationship between skin friction and the pile-soil relative displacement

As mentioned above, the nodular piles and cemented soil around the pile are considered as a whole in the loading process; therefore, the characteristics of the cemented soil are very important for the properties of the composite pile. The water cement ratio of the cement paste is 0.6 to 1.0, which is smaller than the normal water cement ratio, and the cement ratio of the cemented soil is 12% to 20% according to the geological condition. The high quality of the cemented soil makes the relative displacement between the nodular pile and cemented soil to be small. In actual engineering, only the cemented soil-soil displacement should be considered when calculating the pile-soil relative displacement. The relative displacement between the cemented soil and soil can be calculated by (Dong *et al.*, 1994)

$$\delta_i = S - \sum_{j=1}^{i} \frac{L_i}{2}(\varepsilon_j + \varepsilon_{j+1}), \tag{5}$$

where L_i is the length of pile i, S is the pile top settlement, ε_j and ε_{j+1} are strains of the pile at sections j and j+1, respectively.

Fig. 10 shows that the relative displacement at the upper part of the test pile is larger than that at the lower part of the pile, which indicates that the pile-soil relative displacement is gradually mobilized from the top of the pile to the pile tip. The displacement of the test pile increases with the increasing applied load, when the applied load comes to 12000 kN, the settlement of the pile top sharply increases from 53 mm to 87 mm, due to the negligence of staffs, and the axial force of this loading step was not obtained and the pile-soil settlement cannot be calculated; however, according to the regularity of the previous loading step, the punching failure is very likely to occur at the pile tip when loaded to 12000 kN.

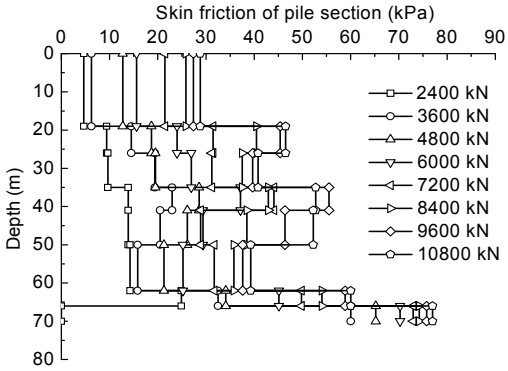

Fig. 9 Skin friction distributions along test pile

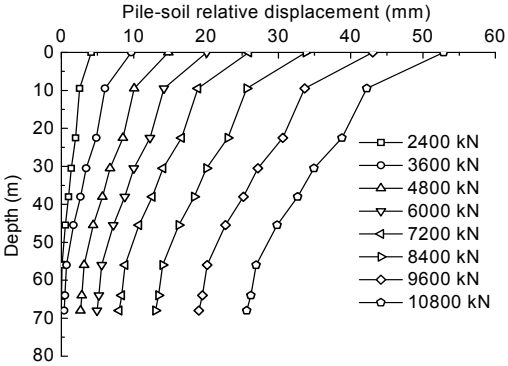

Fig. 10 Pile-soil relative displacement along the test pile

Fig. 11 shows the relationship between the skin friction and pile-soil relative displacement. The skin friction of each soil layer is gradually mobilized with the increase of the pile-soil relative displacement until the skin friction of the soil layer is fully mobilized, then the skin friction of several soil layers will have a small reduction with the increasing pile-soil relative displacement. For bored piles, the pile-soil relative displacement needed to make the skin friction fully mobilized is 6–12 mm for cohesive soil and 8–15 mm for sandy soil in China (Zhang, 2007). While it can be seen in Fig. 11 that the pile-soil relative displacement needed to wholly mobilize the skin friction is 10–20

mm in cohesive soil, which is larger than that of the bored piles. This is probably owing to the fact that the skin friction of the composite pile is provided by the cemented soil-soil interface, and the modulus of the cemented soil is between that of the precast nodular pile and the surrounding soil; therefore, the cemented soil acts as a buffer layer and makes the ultimate pile-soil relative displacement larger. Compared with Fig. 11 and Table 2, it can also be found that the skin friction of the static drill rooted nodular pile is about 1.05–1.10 times larger than that of the bored pile in the same soil layer, and this phenomenon is most obvious in the upper soil layers and inconspicuous in the lower soil layers.

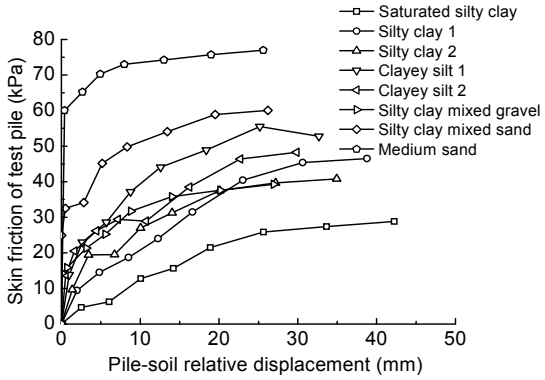

Fig. 11 Skin friction versus pile-soil relative displacement of test pile

3.2.5 Relationship between tip displacement and tip resistance

The relationship between the pile tip displacement and pile tip load is shown in Fig. 12. The pile tip resistance increases sharply with the increasing pile tip displacement at first, then the pile tip resistance curve appears to be linear considering the deviation of the measurement, and then the pile tip load reaches the maximum value 2766 kN when the pile tip displacement is 25.6 mm. As mentioned above the statistics along the pile of the failure stage do not get measured, and no accurate statistic can be obtained. The dotted line in the figure only represents the trend of the curve, and fortunately the maximum value is obtained and it does not make much difference for the analysis. Combining the geological conditions in the field and the standard JGJ94-2008, the ultimate bearing capacity in medium sand is 7500–9000 kPa for a precast concrete pile and 1900–2100 kPa for a bored pile. The area of the precast nodular pile is 0.238 m^2, and the drill diameter at the pile tip is 1.5 times larger than the normal diameter, so the whole diameter of the pile tip is 1.28 m^2, and the calculated value is 2560 kN using bored pile parameters and 2142 kN using the precast concrete pile standards. Therefore, it can be seen that the actual pile tip bearing capacity is larger than the calculated values whether using the precast pile parameters or that of the bored pile. The probable reason is that the injection of the cement paste improves the properties of the surrounding soil and makes the pile tip bearing capacity larger.

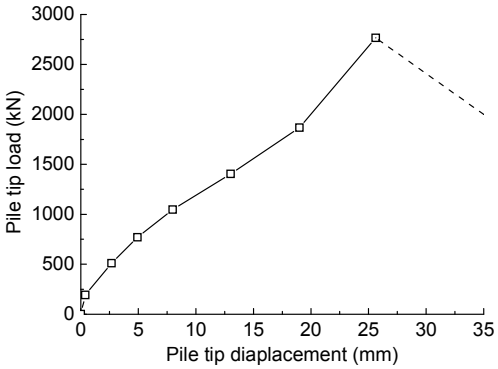

Fig. 12 Pile tip displacement versus pile tip load

4 Finite element method simulation

To provide a more in depth study of the load transfer mechanism of this composite pile, we investigated the load ratio of the precast nodular and cemented soil, and studied the relative displacement between the precast pile and the cemented soil during the loading process. 3D models were built and calculated using the ABAQUS finite element program, for it is difficult to set measuring instruments in the cemented soil in actual engineering.

4.1 Modeling

The 3D model is used to simulate the static drill rooted nodular pile under vertical load, for it is an axisymmetric problem, then a model of half of the composite pile is built. The precast nodular pile is defined as linear elastic material, cemented soil and soil are defined as the Mohr-Coulomb elastoplastic material, the pile-cemented soil relative displacement and cemented soil-soil relative displacement are considered, the initial stress field produced by the

geostatic stress is taken into account, and the applied load is controlled by the displacement control method (Fei and Zhang, 2009). The 72 m long nodular pile is selected to be simulated, and the geometric parameters of the pile are according to the test pile in the field test. The radius of soil around the pile is 20 m in the plane and 100 m in depth, and parameters of the soil are selected according to Table 2. The cement content is 12%–20% in the field test, so the elasticity modulus of the cemented soil is approximately 200 MPa, and Poisson's ratio is 0.3 (Huang *et al.*, 2000). The piling process is relatively fast, and here the total stress analysis and undrained analysis are adopted. The Newton-Raphson iteration method is selected which is commonly used in ABAQUS/STANDARD testing. Details of the soil layers, and parameters of the nodular pile and the cemented soil are listed in Table 3 and Table 4, respectively.

4.2 Interface definition

The selection of the interface element is of great importance in the finite element method modeling, and three interface elements are defined in this model: pile-cemented soil interface, cemented soil-soil interface, and pile-soil interface. The normal contacts of all three interfaces are defined as the hard contact, and the shear contacts are defined as the coulomb friction model. The selection of the friction coefficient is significant for the accuracy of the load transfer process. The friction coefficient of the pile-cemented soil interface is selected to be 0.65 (Wu, 2008). The friction coefficient of the pile-soil interface can be calculated by (Randolph and Worth, 1981):

$$\psi = \arctan\left(\frac{\sin\varphi\cos\varphi}{1+\sin^2\varphi}\right),$$
$$\mu = \tan\psi. \tag{6}$$

The internal friction angle of the pile-soil interface can also be estimated according to (0.75–1)φ (Fei and Zhang, 2009). For normal bored piles, the skin coefficient of the pile-soil interface is 0.25–0.40 in cohesive soil and 0.5–1.0 in sandy soil (Xu *et al.*, 2002).

Zheng and Jiang (1999) pointed out that the skin friction of the cemented soil-soil interface is higher than that of the pile-soil interface of the bored piles. By conducting hundreds of model tests of different soils and materials to study the friction capacity between different soils and materials, Potyondy and Eng (1961) summarized the internal friction angle between different soils and materials. Combining the experience mentioned above with the soil conditions in the test field, the friction coefficient of cemented soil-soil interface is set to 0.3 in cohesive soil and 0.39 in sandy soil. As mentioned above, the normal contacts of the interfaces are defined as hard contact, and the elastic slip allowable value should be set in the elastic slip option, where 0.5% of unit length is commonly used (Fei and Zhang, 2009), so here the elastic slip allowable value is set as 0.5% of the unit length. The sketch of the whole model and nodular pile in the ABAQUS program modeling is shown in Fig. 13.

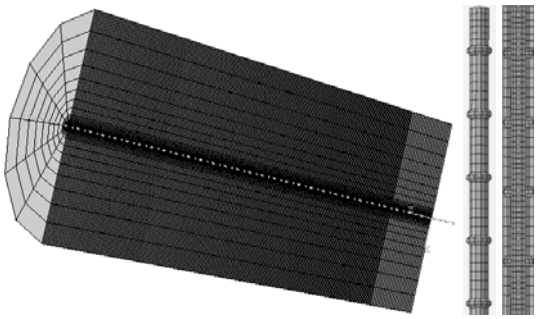

Fig. 13 Sketch of the whole model and nodular pile

Table 3 Parameters of soil layers

Layer No.	Soil layer	γ_{sat} (kN/m^3)	E_s (MPa)	Poisson's ratio	C (kPa)	φ (°)	Thickness (m)
1	Clay	1.8	5	0.40	20	25	20
2	Silty clay	1.8	20	0.38	35	30	50
3	Medium sand	1.9	30	0.36	10	35	30

Table 4 Parameters of nodular pile and cemented soil

Name	E_s (MPa)	Poisson's ratio	C (kPa)	φ (°)	Thickness (m)
Pile	45000	0.15			72
Cemented soil	2000	0.3	200	35	72

4.3 Analysis of the results

The simulation calculation starts after the modeling process is completed, and the load-displacement curves of the field test and that calculated by ABAQUS program are shown in Fig. 14.

It is shown in Fig. 14 that the load-displacement curve calculated by ABAQUS has some differences with the load-displacement curve of the field test, yet the trends of the two curves are similar and the ultimate bearing capacity of the two curves are close, which indicates that the proposed modeling method is reliable and it is feasible to use this model to investigate the load transfer mechanism of static drill rooted nodular piles.

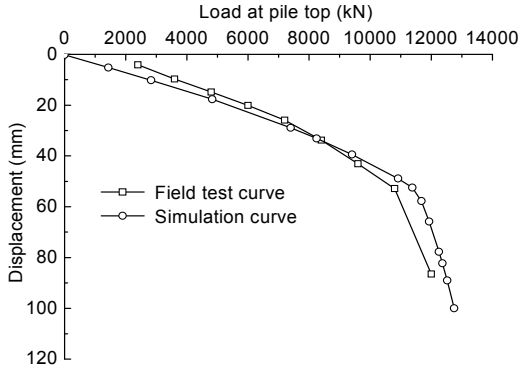

Fig. 14 Load-displacement curves of 850 mm nodular pile of the field test and that calculated by ABAQUS

4.4 Simulation of destructive field tests

In order to validate the reliability of the modeling method, the composite pile in the destructive field test mentioned in Section 1 is simulated as well. Modeling steps are the same as that in Section 3.1: a 850 mm nodular pile in the destructive field test is selected to be simulated, and the geometric parameters of the pile are the same as the test pile in the destructive field test. The friction coefficient of the pile-cemented soil interface is also set to be 0.65, combined with the soil conditions in the test place, the friction coefficient of cemented soil-soil interface is set as 0.36 in the cohesive soil and 0.40 in the sandy soil, and the elastic slip allowable value is also set as 0.5% of the unit length. The load-displacement curves of the destructive field test and that calculated by the ABAQUS program are shown in Fig. 15.

Fig. 15 shows that the load-displacement curve calculated by ABAQUS is similar to that in the destructive field test except that for some dissimilarities in settlement which do not make a big difference, the ultimate bearing capacity of the two curves are almost the same. Therefore, the result also shows that the proposed modeling method is reliable.

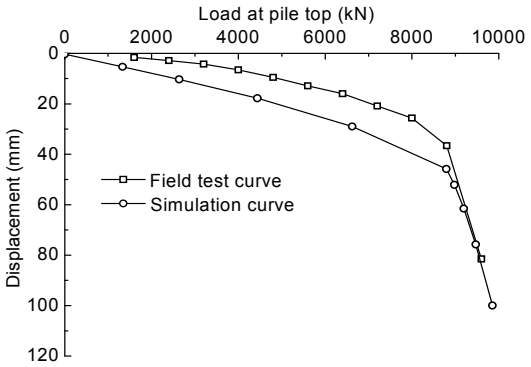

Fig. 15 Load-displacement curves of nodular pile of the field test and that calculated by ABAQUS

4.5 Load ratio of nodular pile and cemented soil

The axial force of the precast pipe pile and the nodular pile can be measured with strain gauges in the field test; however, it is difficult to measure the axial force of the cemented soil around the pile. As an important part of the composite pile, research on the properties of cemented soil during the loading process is of great significance. Therefore, the statistics of ABAQUS modeling are used to give a deeper study of this composite pile, and the 72 m nodular pile in the field test is analyzed in this study.

The distribution of the axial force of the precast pile is shown in Fig. 16 and the distribution of the axial force of the cemented soil is shown in Fig. 17. As the finite element calculation is not easy to converge in consideration of the length of the pile and the existence of the nodes along the nodular piles, the length of the calculation step is not set and it has no regularity during the calculation process; therefore, four steps are selected to investigate the load transfer mechanism of this composite pile when the settlement of the pile top reaches 10 mm, 28.75 mm, 45.63 mm, and 100 mm.

As shown in Fig. 16, the trend of the axial force of the precast pile along the pile is consistent with the actual situation. Fig. 16 also shows that the curves are smooth at the upper part of the pile and have turning points at the lower part of the pile. The axial force of the pile decreases sharply when passing the nodes, which is probably due to the fact that the cross section

at the node is larger than that at other parts and the contact area between the pile and cemented soil is also larger. Stress mutation is very likely to occur at the node of the nodular pile because of the change of the cross section. The stress mutation of the pile is shown in Fig. 18a, where only a section of the pile is selected to make the phenomenon be easily seen as the pile is too long.

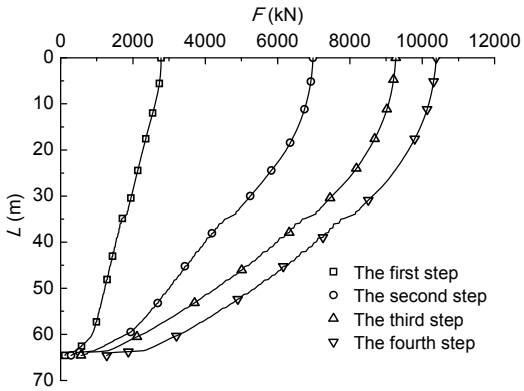

Fig. 16 Axial force of nodular pile calculated by ABAQUS

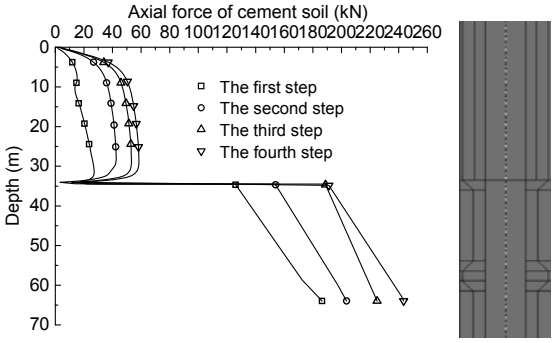

Fig. 17 Axial force of cemented soil calculated by ABAQUS and sketch of cemented soil on variable cross-section

The distribution of the axial force of the cemented soil is different from that of the nodular pile (Fig. 17). The load is applied on the precast pile in the model, and the axial force of the cemented soil gradually increases along the pile, then the axial force of the cemented soil decreases after passing 30 m deep, and the axial force increases at a larger scale at a depth of 34 m where the precast nodular pile takes place in the pipe pile. This is probably because the diameter of the pipe pile is 800 mm while the diameter of the nodular pile is 600 m, and the diameter of the cemented soil is 850 mm along the whole pile, so the thickness of the cemented soil increases and leads to the increase of the axial force of the cemented soil. In addition, the geometrical shape changes at this cross section which may lead to stress concentration, which can also make the axial force of the cemented soil to increase. Therefore, the strength of the cemented soil at this cross section should be pay attention to in actual engineering. The stress mutation phenomenon also occurs in the cemented soil as shown in Fig. 18b. As the stress of the cemented soil shocks along the nodular pile part, the average value of the stress of the cemented soil is selected to show the variation trend of the axial force of the cemented soil. It can also be seen in Fig. 17 that the axial force of the cemented soil gradually increases at a smaller scale. To ensure that the cemented soil should not be broken during the loading process, the strength of the cemented soil should be checked. The maximum force on the cemented soil is 240 kN, the minimum cross section is 0.065 m^2, the strength is 3.7 MPa, and the compressive strength of the cemented soil in this

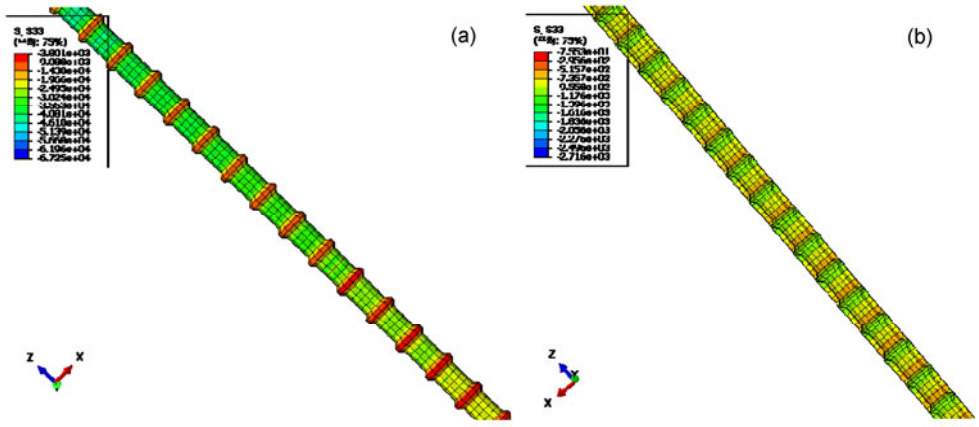

Fig. 18 Stress mutation on the nodes of nodular pile (a) and cemented soil (b)

actual engineering is about 5 MPa, so the cemented soil is reliable in this engineering.

Comparing Fig. 16 with Fig. 17, it can be seen that the axial force of the cemented soil is much smaller than that of the precast pile, which indicates that the load supported by the cemented soil can be ignored. Therefore, the cemented soil mainly plays the role of transmitting the load from the precast pile to the surrounding soil. Consequently, the static drill rooted nodular pile has a double stress dispersion system: the applied load on the precast pile is firstly delivered to the cemented soil as well as passed on to the lower part, and then the load is delivered to the surrounding soil through the cemented soil-soil interface. It has been demonstrated in the destructive field tests that the bearing capacity of the static drill rooted nodular piles is higher than the bored piles in the soft soil areas, so that the double stress dispersion system is probably better than a traditional load transfer system in soft soil areas.

4.6 Pile-cemented soil relative displacement

As a kind of composite pile, the precast nodular pile and the cemented soil should always be a whole during the loading process, so the deformation of the nodular pile and cemented soil should be considered as deformation compatible. The pile-cemented soil relative displacement is shown in Fig. 19.

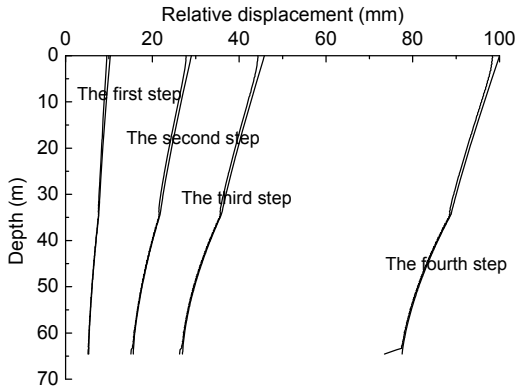

Fig. 19 Pile-cemented soil relative displacement curves under different loads

Fig. 19 shows that the pile-cemented soil relative displacement is the largest at the top of the pile and decreases along the pile before being stopped at a stable state, for the load is applied on the precast pile. The displacement differences of the precast pile and cemented soil at the top of the composite pile are 8.1%, 4.3%, 3.4%, 1.7%, respectively for the four steps, which indicates that the displacement of the composite pile is controlled by the precast nodular pile and the precast pile and cemented soil around the pile can be considered as a whole during the loading process. Fig. 18 also shows that the displacement curves of the precast pile and cemented soil appear as one after reaching a depth of 34 m, as mentioned above the pipe pile is replaced with a nodular pile at the depth of 34 m, so it can be demonstrated that the adhesive effect between the nodular pile and cemented soil is better than that between the pipe pile and cemented soil. The pile-cemented soil displacement increases at the pile tip, and the phenomenon is more obvious when the displacement of the pile top reaches 100 mm and the punching failure happens. The possible reason is that the cemented soil at the pile tip is destroyed and the cemented soil and precast pile is separated at the pile tip; therefore, the pile-cemented soil displacement is relatively large when the punching failure occurs at the pile tip.

4.7 Comparison of bearing capacity between nodular pile and bored pile

In destructive field tests, the most commonly used types of bored piles and static drill rooted nodular piles are selected, so 800 mm bored piles are compared with 700 mm static drill rooted nodular piles, and 1000 mm bored piles are compared with 850 mm static drill rooted nodular piles, making the diameters of the compared piles to be different. In order to investigate the bearing capacity between two types of piles of the same diameter, ABAQUS is adopted to simulate two kinds of piles with the same diameter. The 800 mm bored pile and the 1000 mm bored pile are simulated for demonstrating that the proposed modeling method is reliable. The load-displacement curves of the field test and the calculation by the ABAQUS program are shown in Fig. 20 and Fig. 21, respectively. The curves of the field tests and that calculated by ABAQUS are similar and the ultimate bearing capacities of each of the compared curves are close, which indicates that the proposed modeling method can also be used to simulate the bored piles.

To compare the bearing capacity of 850 mm bored pile and 850 mm static drill rooted nodular pile, the 1000 mm bored pile in the model is changed to

850 mm bored pile. Parameters of the precast pile, cemented soil and soil, and the properties of the pile-soil interface are the same as that of the 1000 mm bored pile model, and the load-displacement curves of the 850 mm bored pile and 850 mm static drill rooted nodular pile calculated by ABAQUS are shown in Fig. 22.

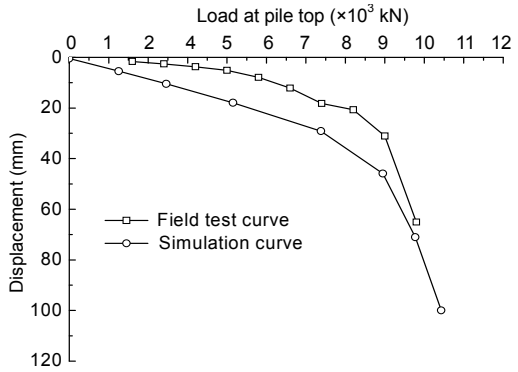

Fig. 20 Load-displacement curves of 800 mm bored pile of destructive field test and that calculated by ABAQUS

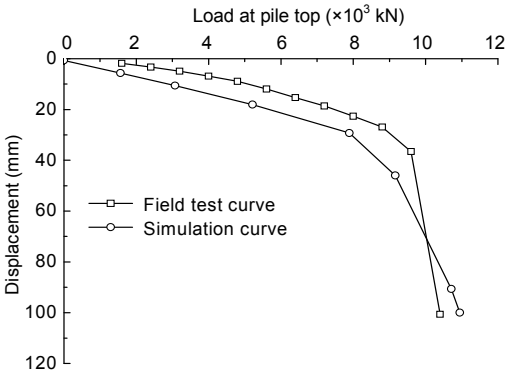

Fig. 21 Load-displacement curves of 1000 mm bored pile of destructive field test and that calculated by ABAQUS

Fig. 22 shows that the load-displacement curves of the two piles almost coincide at the beginning of the loading process, yet the ultimate bearing capacity of the 850 mm static drill rooted nodular pile is 8.5% larger than that of the 850 mm bored pile, which indicates that the bearing capacity of the static drill rooted nodular piles is higher than that of the bored piles.

The distribution of the axial force of the bored pile and nodular pile is shown in Fig. 23. It can be seen in Fig. 23 that the pile top axial force of the 850 mm static drill rooted nodular pile is larger than the axial force of the 850 mm bored pile while the pile tip axial force of the nodular pile is smaller than that of the bored pile, which indicates that the skin friction of the static drill rooted nodular pile is larger than that of the bored pile with the same diameter and the same soil conditions. Therefore, the cemented soil-soil interface can be determined to be better than the pile-soil interface of the bored piles in soft soil areas, which is consistent with the conclusion raised in Section 3.2.4 that the skin friction of the static drill rooted nodular pile is larger than that of the bored pile in the same soil layer.

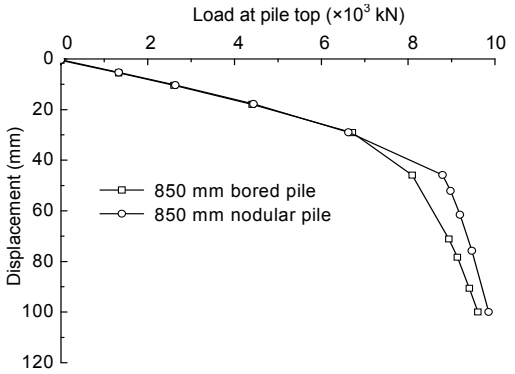

Fig. 22 Load-displacement curves of 850 mm bored pile and 850 mm nodular pile that calculated by ABAQUS

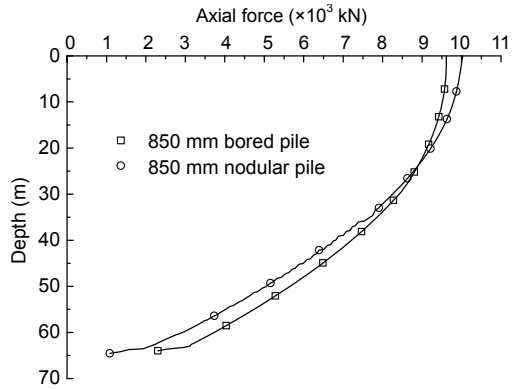

Fig. 23 Axial force of bored pile and nodular pile along the pile

5 Conclusions

This paper investigates the bearing capacity and load transfer mechanism of a static drill rooted nodular pile through a series of field tests and ABAQUS modeling, and some conclusions can be drawn:

1. According to the field tests and the numerical analysis, the bearing capacity of the static drill rooted nodular pile is about 8% to 10% higher than that of the bored pile in the soft soil areas. Statistics from the

primary applications in some places of the deep soft soil layers in China show that the cost can be decreased by 10% using this nodular pile compared to the bored piles.

2. The static drill rooted nodular pile combines the advantages of the relatively high skin friction of the cemented soil pile and the higher strength of the precast pile, and a double stress dispersion system is formed. From the field test, this load transfer system proves to be better than that of traditional piles in the soft soil areas. Moreover, the mud pollution is greatly decreased by using this method.

3. The settlement of the static drill rooted nodular pile is controlled by the precast nodular pile. The maximum displacement differences of the precast pile and cemented soil are 8.1%, 4.3%, 3.4%, 1.7%, respectively for the four steps in the numerical analysis, so the nodular pile and cemented soil can be considered as deformation compatible.

4. The nodes on the nodular pile play an important role during the load transfer process. The axial load of the nodular pile will decrease sharply when passing the node, and the settlement curves of the nodular pile and cemented soil are almost coincident in this part of the nodular piles.

5. According to the field test, the skin friction of the static drill rooted pile is about 1.05–1.10 times higher than that of the bored pile in the soft soil layer.

References

Borda, O., Uno, M., Towhata, I., 2007. Shaft Capacity of Nodular Piles in Loose Sand. Proceedings of the 49th National Conference, Japanese Geotechnical Society, **2**:1175-1176 (in Japanese).

Dong, J.R., Lin, S.T., Dai, Y.M., 1994. The load transfer behavior of large diameter cast-in-situ pile in crushed pebble stratum. *Chinese Journal of Geotechnical Engineering*, **16**(6):123-131 (in Chinese).

Dong, P., Qin, R., Chen, Z.Z., 2004. Bearing capacity and settlement of concrete-cored DCM pile in soft ground. *Geotechnical and Geological Engineering*, **22**(1):105-119. [doi:10.1023/B:GEGE.0000013994.73567.cc]

Fei, K., Zhang, J.W., 2009. ABAQUS in Geotechnical Engineering. China Water Power Press, Beijing (in Chinese).

Honda, T., Hirai, Y., Sato, E., 2011. Uplift capacity of belled and multi-belled piles in dense sand. *Soils and Foundations*, **51**(3):483-496.

Horiguchi, T., Karkee, M.B., 1995. Load tests on bored PHC nodular piles in different ground conditions and the bearing capacity based on simple soil parameters. *Proceedings of Technical Report of Japanese Architectural Society*, **1**:89-94 (in Japanese).

Huang, H., Zhang, L., Yang, X.Q., 2000. Experimental study of the mechanical properties of the cemented soil material. *Taiyuan University of Technology*, **36**(6):705-709 (in Chinese).

JGJ106-2003. Building Pile Testing Technology Code. Ministry of Housing and Urban-rural Development, China (in Chinese).

JGJ94-2008. Technical Code for Building Pile Foundations. Ministry of Housing and Urban-rural Development, China (in Chinese).

Karkee, M.B., Kanai, S., Horiguchi, T., 1998. Quality Assurance in Bored PHC Nodular Piles Through Control of Design Capacity Based on Loading Test Data. Proceedings of the 7th International Conference and Exhibition, Piling and Deep Foundations, Vienna, Austria, **1**(24):1-9.

Petros, P.X., Lee, W.A., Donald, A.B., 1994. Ground Control and Improvement. John Wiley & Sons Inc., New York.

Potyondy, J.G., Eng, M., 1961. Skin friction between various soils and construction materials. *Geotechnique*, **11**(4): 339-353. [doi:10.1680/geot.1961.11.4.339]

Randolph, M.F., Worth, C.P., 1981. Application of the failure state in undrained simple shear to the shaft capacity of driven piles. *Geotechnique*, **31**(1):143-157. [doi:10.1680/geot.1981.31.1.143]

Wang, J., Xia, M.Y., Fu, D.M., 1998. Design and calculation of composite structure with H shaped steel and cemented-soil-pile. *Journal of Tongji University (Natural Science)*, **26**(6):636-639 (in Chinese).

Wu, M., 2008. Research on Vertically Bearing Behavior and Reliability Analysis of Concrete-cored DCM Pile. PhD Thesis, Tianjin University, China (in Chinese).

Xu, H.F., Wu, H.J., Guo, S.P., 2002. Study on the parameters of pile soil contact surface element. *Exploration Engineering*, (5):10-12 (in Chinese).

Yabuuchi, S., 1994. Bearing Mechanisms of Multi-node Piles. Proceedings of the International Offshore and Polar Engineering Conference, **1**:504-507.

Zhang, Z.M., 2007. Pile Foundation Engineering. China Architecture and Building Press, Beijing, p.72-84 (in Chinese).

Zheng, G., Jiang, X.L., 1999. Research on the bearing capacity of cement treated composite foundation. *Rock and Soil Mechanics*, **20**(3):46-50 (in Chinese).